Revisiting Rb2TiNb6O18 as electrode materials for energy storage devices

Jeronimo Miranda, Etienne Le Calvez, Richard Retoux, Olivier Crosnier, Thierry Brousse

Electrochemistry Communications 137 (2022) 107249

Contents lists available at ScienceDirect

Electrochemistry Communications

journal homepage: www.elsevier.com/locate/elecom

Revisiting $Rb_2TiNb_6O_{18}$ as electrode materials for energy storage devices

Jeronimo Miranda [a,b], Etienne Le Calvez [a,b], Richard Retoux [c], Olivier Crosnier [a,b], Thierry Brousse [a,b,*]

[a] Nantes Université, CNRS, Institut des Matériaux de Nantes Jean Rouxel, IMN, F-44000 Nantes, France
[b] Réseau sur le Stockage Électrochimique de l'Énergie (RS2E), CNRS FR 3459, 33 rue Saint Leu, 80039 Amiens Cedex, France
[c] CRISMAT-CNRS/UMR 6508, ENSICAEN Université de Caen Basse-Normandie Caen, 14050 Cedex 4, France

ARTICLE INFO

Keywords:
Lithium-ion battery
High rate electrode
Negative electrode
Tunnel structure
Titanium niobiate

ABSTRACT

In the search of new materials for the future generation of Li-ion batteries, a look into the past has brought the multicationic oxide $Rb_2TiNb_6O_{18}$ to the foreground. Structural characterization of this material has been carried out thanks to the combination of XRD, SEM and HRTEM highlighting the complex structure of this material. Ion exchange was performed in order to replace the rubidium ions by hydrated protons. Then, a comparative study of $Rb_2TiNb_6O_{18}$ and the obtained proton exchanged analogues $H_2TiNb_6O_{18}$ when used as negative electrode materials is depicted in terms of both structure and electrochemical behavior. Interestingly, while only a negligible Li^+ insertion is evidenced in the rubidium phase, the $H_2TiNb_6O_{18}$ exhibits a much higher lithium intercalation between 1 V and 3 V *vs* Li/Li^+. A specific capacity of 118 $mAh.g^{-1}$ is reported when cycled at 0.02 $A.g^{-1}$. A solid solution type mechanism has been revealed by *in situ* XRD experiments. Moreover, during the lithiation, the volume of the material increases by only 1% showing the interest of this type of phase to develop "zero-strain" materials.

1. Introduction

For a wider development of low-carbon mobility via electric cars, the synthesis of materials with the ability to charge quickly appears to be an essential point.[1–3] Graphite, the most commercially used negative electrode material, is not in line with this perspective. Despite a relatively large theoretical specific capacity of 372 $mAh{\cdot}g^{-1}$ for graphite based electrodes, the reduction of Li^+ to Li^0 can occur at a potential down to 0 V *vs.* Li/Li^+ during the charging step of graphite at high current densities, leading to a metallic dendritic growth of metallic lithium on the surface of graphite, that could cause possible overheating and short circuits.[4,5] Additionally, the formation of a solid electrolyte interface (SEI) passivates the graphite surface, which slows down the transfer of Li^+ to and from the electrolyte, also lowering the power capabilities of graphite. Therefore, for LIBs to compete in the world of fast charging electrochemical devices, alternative negative electrode materials have been proposed and investigated.[6–9] In fact, the extension of LIBs into high-power applications can only be achieved if the undesired side reactions of Li^+ on the surface of the negative electrode are prevented at high rates. A practical solution to this challenge has been to find redox-active materials where Li^+ insertion occurs at a potential far away from the thermodynamic reduction of Li^+ (i.e., E greater than 1.0 V *vs.* Li/Li^+) in order to avoid lithium plating but also SEI formation which decreases the power ability of electrodes and classically appears at a potential close to 0.8 V *vs* Li/Li^+.[7,8,10,11] In this case, a classic example is T-Nb_2O_5 which show reversible Li^+ intercalation between 1.0 V and 2.0 V *vs* Li/Li^+ with an extremely good capacity retention even at high rates over 20C[12,13].

In their extensive work on Nb-based polycationic materials, Raveau et al.[14–17] reported a different kind of tunneled Nb-based oxides showing pre-occupied cages. Large cationic species (i.e., K^+, Rb^+, Cs^+, Tl^+) are originally located within the cages of the material, stabilizing large interconnected hexagonal tunnels. Interestingly, remarkable cationic exchange behavior has been reported in some of these materials.[15,16] Consequently, the displacement of the original large alkali cations by smaller species (H^+, Li^+, …) can liberate part of the accessible volume within the hexagonal channels, without triggering any phase change in the material.

$Rb_2Nb_6TiO_{18}$, exhibits an interconnected bronze-like tunnel structure, as well as the presence of possible Nb^{5+} and Ti^{4+} active redox centers. In this case, no ionic exchange properties were previously reported. In this work, for the first time, protonated substituted

* Corresponding author at: Nantes Université, CNRS, Institut des Matériaux de Nantes Jean Rouxel, IMN, F-44000 Nantes, France.
E-mail address: thierry.brousse@univ-nantes.fr (T. Brousse).

https://doi.org/10.1016/j.elecom.2022.107249

Available online 25 February 2022

$Rb_2Nb_6TiO_{18}$ and consequent electrochemical characterization as LIB negative electrode material are reported. Both structural and electrochemical differences between $Rb_2TiNb_6O_{18}$ and $H_2TiNb_6O_{18}$ are discussed in the following parts of this communication.

2. Experimental section

2.1. Synthesis of $Rb_2TiNb_6O_{18}$ / $H_2TiNb_6O_{18}$

High-temperature solid state methods were used to synthesize $Rb_2TiNb_6O_{18}$. Stoichiometric amounts of Nb_2O_5 (Alfa Aesar, 99.9% metal basis), TiO_2 and 10% excess Rb_2CO_3 (ACROS Organics 99%) were thoroughly mixed using an agate mortar and pestle. The powdered mixture was heated at 900 °C for 6 h followed by re-grinded and a final calcination at 1150 °C using a platinum crucible for 12 h. The phase purity of the resulting materials was checked by X-ray diffraction and Le Bail refinement.

Protonated substituted phases were obtained by introducing the powder samples in 3 M HCl (Fisher bioreagent, analytical reagent grade) for 3 days upon stirring. Substitution was performed at 100 °C, by regularly add the 3 M HCl solution. Substitution amounts were estimated by EDX by means of comparing experimental Nb/Rb ratios to the theoretical one of $Rb_2TiNb_6O_{18}$.

2.2. Characterization

2.2.1. Powder X-ray diffraction

Powder XRD data was collected using a PANalytical X'Pert Pro diffractometer with using a Cu source ($K\alpha_1 = 1.5406$ Å, $K\alpha_2 = 1.5444$ Å) and K_β filter (Nickel) in the Bragg-Brentano reflection geometry. Data was collected from 10 to 90° 2θ. *In situ* electrochemical cycling XRD was obtained using a lab-produced cell, close to "Letiche cell" using a Beryllium window and by cycling the cell at 0.005 $A.g^{-1}$ with 30 min at open circuit voltage for XRD pattern collection.[18] All XRD were collected in ~ 0.008° 2θ steps. Structure refinement has been performed using FullProf Suite. Preliminary values of this refinement have been taken from the literature.[14]

2.2.2. Thermogravimetric analysis (TGA)

TGA was performed using a TA 449 F3 Jupiter device. Samples (50–100 mg) were stabilized at 50 °C for 20 min followed by 3 °C.min^{-1} temperature ramp from 50 to 700 °C in argon-flow mode.

2.2.3. SEM and TEM

SEM micrographs were obtained at 20 kV using a Zeiss MERLIN Instrument using in-Lens annular detector. Samples were prepared by dispersing a small fraction of the powder on a piece of conducting carbon tape. EDX was collected at 8.0 mm working distance using an X-Max 50 mm^2 OXFORD Instruments detector. TEM observations were performed using a 200 kV JEOL F200 Cold FEG Transmission Electron Microscope, fitted with a ± 35° double tilt sample holder and a EDX JEOL centurion XL (Energy Dispersive X-ray detector).

2.2.4. Electrochemistry

Electrodes were prepared by thoroughly grinding active material, conducting carbon (Superior graphite) and polyvinylidene fluoride (PTFE) binder (Sigma-Aldrich, 60 wt% dispersion in H_2O) in a 75:15:10 wt ratio, with about 2 mL of ethanol, until a paste was obtained. The paste was rolled out to a thickness of ~ 150 μm using a glass cylinder. Electrodes were dried at 60 °C overnight before cutting them into 12 mm diameter disks using a manual electrode puncher. Resulting electrodes ranged between 5 and 10 $mg{\cdot}cm^{-2}$, consistent with reasonable mass loading metrics.[19] Electrochemical experiments were performed using Swagelok cells in a 2-electrode configuration. Cells were mounted inside an Argon-filled glovebox (<0.1 ppm O_2, H_2O) using a single lithium (Li) electrode as both reference and counter (99.9%, Sigma Aldrich), glass fiber separator (Whatman) and 200 μL of 1 M $LiPF_6$ in ethylene carbonate/dimethyl carbonate (EC/DMC) 1:1 v/v (Solvionic, 99.9% purity, electrochemistry grade) as the electrolyte.

All electrochemical studies were performed using a MPG2 BioLogic Potentiostat/Galvanostat controlled by EC-Lab Software. Cyclic voltammetry (CV) were collected at 2 $mV{\cdot}s^{-1}$. Galvanostatic cycling with potential limitation (GCPL) cycling was performed in series of 5 cycles at 0.02, 0.05, 0.10, 0.20, 0.50, 1.00 $A{\cdot}g^{-1}$. The charge–discharge curves presented in the respective figures correspond always the third charge/discharge curve out of the five.

3. Results & discussion

The crystallographic structure of $Rb_2TiNb_6O_{18}$ is presented in Fig. 1.A. The material crystallizes in the hexagonal system, with a P $\bar{3}$ m1 space group. The structure is composed of two types of distorted $(Nb/Ti)O_6$ octahedra sharing corners and edges. More precisely, $Rb_2TiNb_6O_{18}$ are formed by the intergrowth of $(M_6O_{15})_n$ and $(MO_3)_n$ layers which creates the 3D structure and cages. As previously reported[20], Ti cations seem to be preferentially located in the (MO_3) sites due to a lower distortion of these octahedra. Rb^+ is located within large O_{21} cages (158.7 $Å^3$) which is formed in the bronze-like hexagonal tunnels interconnected along [1 0 0], [0 1 0] and [1 1 0] directions.

The purity of the phase was confirmed by Le Bail refinement shown in Fig. 1.B. Unit cell parameters were determined as $a = 7.5323(5)$ Å and $c = 8.2002(6)$ Å, showing a very small difference with the previously reported values. [14,20] A SEM micrograph in Fig. 1.C shows that large particles of ~ 10 um were obtained, as expected from the high-temperature conditions of the synthesis process. HR-TEM micrographs in Fig. 1.(D-E) reveal some differences between (1 1 0) and (1 0 1) planes. While large homogenous domains are observed on (1 1 0) plane, some defects are visible along (1 0 1). This observation might be a result of Ti deficiency located in the (MO_3) sites, causing some irregularities in the stacking sequence of the layers and then local rearrangement of the structure. Nevertheless, the HRTEM images along with (1 1 0) and (1 0 1) planes highlight the presence of cages along these directions.

The substitution of Rb^+ ions by H^+ ions, as described in the experimental part, was checked by EDX. A ratio of 1 for 40 between Rb and Nb allows us to assume that a nearly complete substitution by protons is achieved. Meanwhile, a Nb/Ti ratio remains at a value close to 6, as expected, before and after proton exchange. Diffractograms of both $Rb_2TiNb_6O_{18}$ and $H_2TiNb_6O_{18}$ are shown in Fig. 2.A. Interestingly, no phase change is observed and both materials get very close cell parameters. A small decrease from 7.5323(5) to 7.5126(5) Å for the *a* parameter and from 8.2002(6) to 8.1807(7) Å for the *c* parameter is observed. $H_2TiNb_6O_{18}$ shows slightly smaller parameters because of the replacement of bulky Rb^+ by a smaller cation. Nevertheless, as reported in some similar substitutions[15,16], the proton is inserted into the structure accompanied by a water molecule with no difference in terms of particle size nor cristallinity.[21–24] Subsequently, a TGA was performed and the associated results are shown in Fig. 2.B. About 4% of the mass is lost between 50 °C and 700 °C which corresponds to 2 water molecules per cell unit, as observed in the literature [14–16]. Thus, we can conclude that during the ionic exchange, about one H_2O molecule per proton is inserted in $H_2TiNb_6O_{18}{\cdot}2H_2O$

To investigated the electrochemical activity of both $Rb_2TiNb_6O_{18}$ and $H_2TiNb_6O_{18}{\cdot}2H_2O$, CVs were performed at 2 $mV{\cdot}s^{-1}$ between 3 V and 1 V *vs* Li/Li^+. As shown in Fig. 3.A, $Rb_2TiNb_6O_{18}$ shows a weak electrochemical signature within the investigated potential range, only a weak double layer capacitance is observed corresponding to a capacity of about 13 $mAh.g^{-1}$. In fact, due to the steric gene created by the presence of the bulky and not mobile Rb^+ ions, no insertion of Li^+ ions in the O_{21} cages are possible. In contrast to his Rb^+ analogue, $H_2TiNb_6O_{18}{\cdot}2H_2O$ has a clear faradic electrochemical signature. A broad wave between 2.6 and 1.5 V *vs.* Li/Li^+ probably arises from the combination of

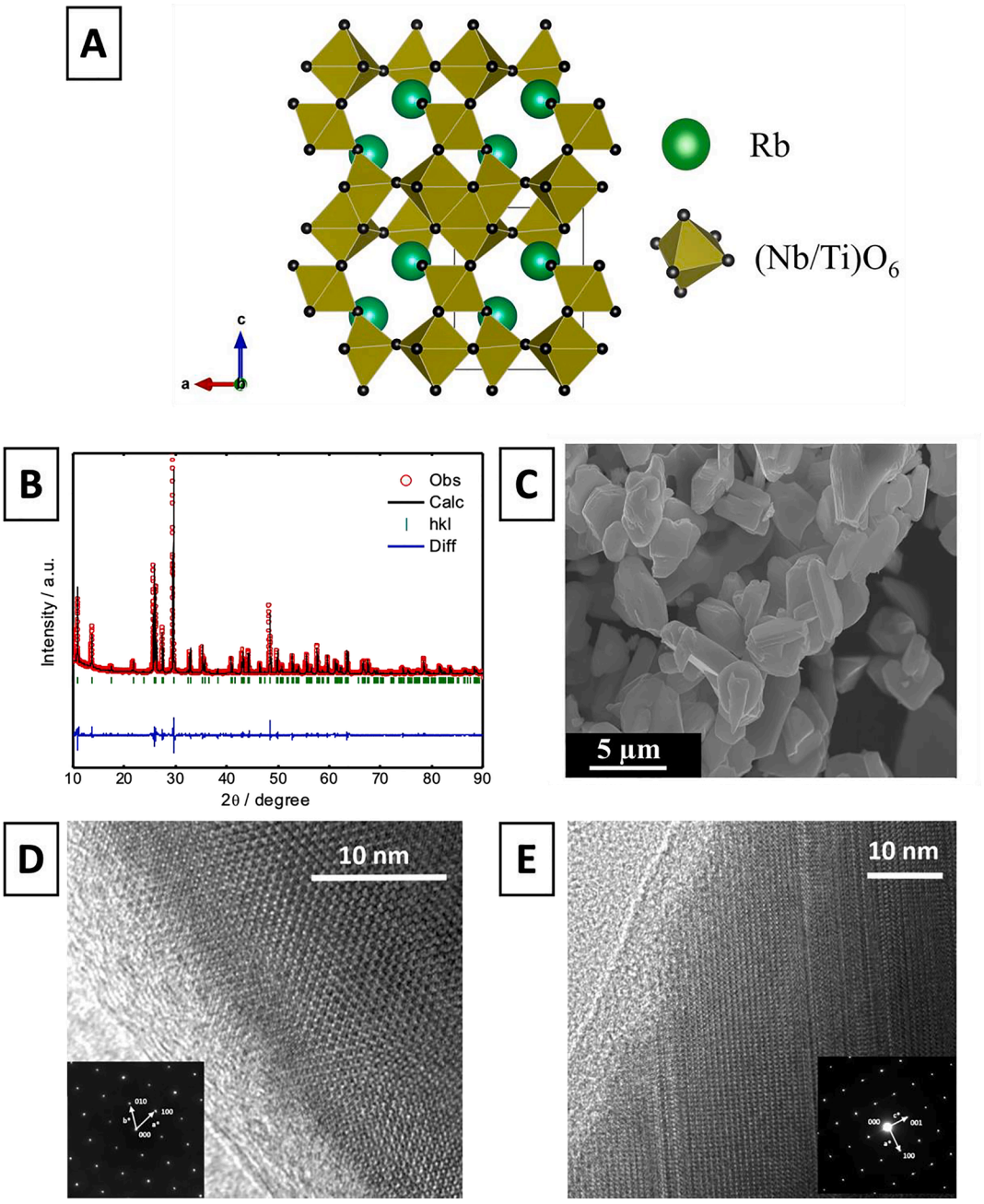

Fig. 1. A. Crystal structure of 2x2 $Rb_2TiNb_6O_{18}$ unit cell. (space group P $\bar{3}$ m1) B. Full pattern matching refinement of $Rb_2TiNb_6O_{18}$. Rwp = 37.5 % / Chi^2 = 13.6. C. SEM image of $Rb_2TiNb_6O_{18}$. D. (1 1 0) plane of $Rb_2TiNb_6O_{18}$ observed by TEM. E. (1 0 1) *plane* of $Rb_2TiNb_6O_{18}$ observed by TEM.

several superimposed redox activities, such as the irreversible reduction of structural water, and the reduction of Nb and/or Ti upon Li^+ insertion. Similarly, a final wave below 1.3 V *vs.* Li/Li^+ suggests a further reduction of the metal hosts at this lower potential. After 5 cycles, the remaining specific capacity is 100 $mAh.g^{-1}$ at 2 $mV{\cdot}s^{-1}$. The reversible reduction of the Nb^{5+}/Nb^{4+} and/or Ti^{4+}/Ti^{3+} redox couples is most probably at the origin of the charge transfer observed in this material upon cycling, as described in the literature.[25] We can conclude from CV experiments that substitution of rubidium by protons give to this oxide the ability to significantly store more lithium ions into its structure.

Based on the obvious differences in CV between $Rb_2TiNb_6O_{18}$ and $H_2TiNb_6O_{18}{\cdot}2H_2O$, the rate capability of these two materials was investigated by GCPL cycling at increasing current densities. Results are shown in Fig. 3(C-D). As expected, the Li^+ insertion in the O_{21} cages is very low for $Rb_2TiNb_6O_{18}$ at every measured current density. Once again, in contrast, $H_2TiNb_6O_{18}{\cdot}2H_2O$ presents a reversible specific capacity of 118 $mAh.g^{-1}$ at 0.02 $A.g^{-1}$, which corresponds to more than $3.55Li^+$ inserted/unit cell. It is 4 times higher than the capacity observed for $Rb_2TiNb_6O_{18}$ in the same conditions. $H_2TiNb_6O_{18}{\cdot}2H_2O$ inserts its lithium ions between 1.8 V and 1.0 V with a linear slope. This "pseudo-capacitive like" signature can be linked to the presence of various insertion sites with different activation energies in the structure which allows a practically constant Li^+ insertion rate between 1.8 and 1.0 V *vs* Li/Li^+. Further study of the electrochemical behavior of the electrode is under progress.

Nevertheless, when the current density is increased, the specific capacity of $H_2TiNb_6O_{18}{\cdot}2H_2O$ sharply decreases. At 0.2 $A.g^{-1}$, a specific capacity of 32 $mAh.g^{-1}$ is observed which represented 27 % of the capacity at 0.02 $A.g^{-1}$. This relatively poor electrochemical behavior at

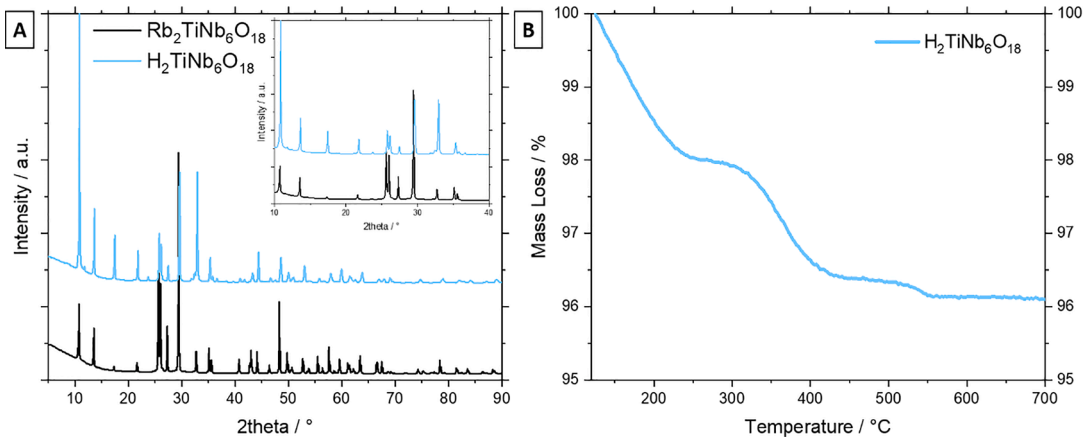

Fig. 2. A. X-ray diffraction patterns of $Rb_2TiNb_6O_{18}$ and $H_2TiNb_6O_{18}$ indexed in P $\bar{3}$ m1 space group. B. TGA curves between 40 °C and 700 °C of $H_2TiNb_6O_{18}$ showing the number of structural water molecule (one water molecule per proton).

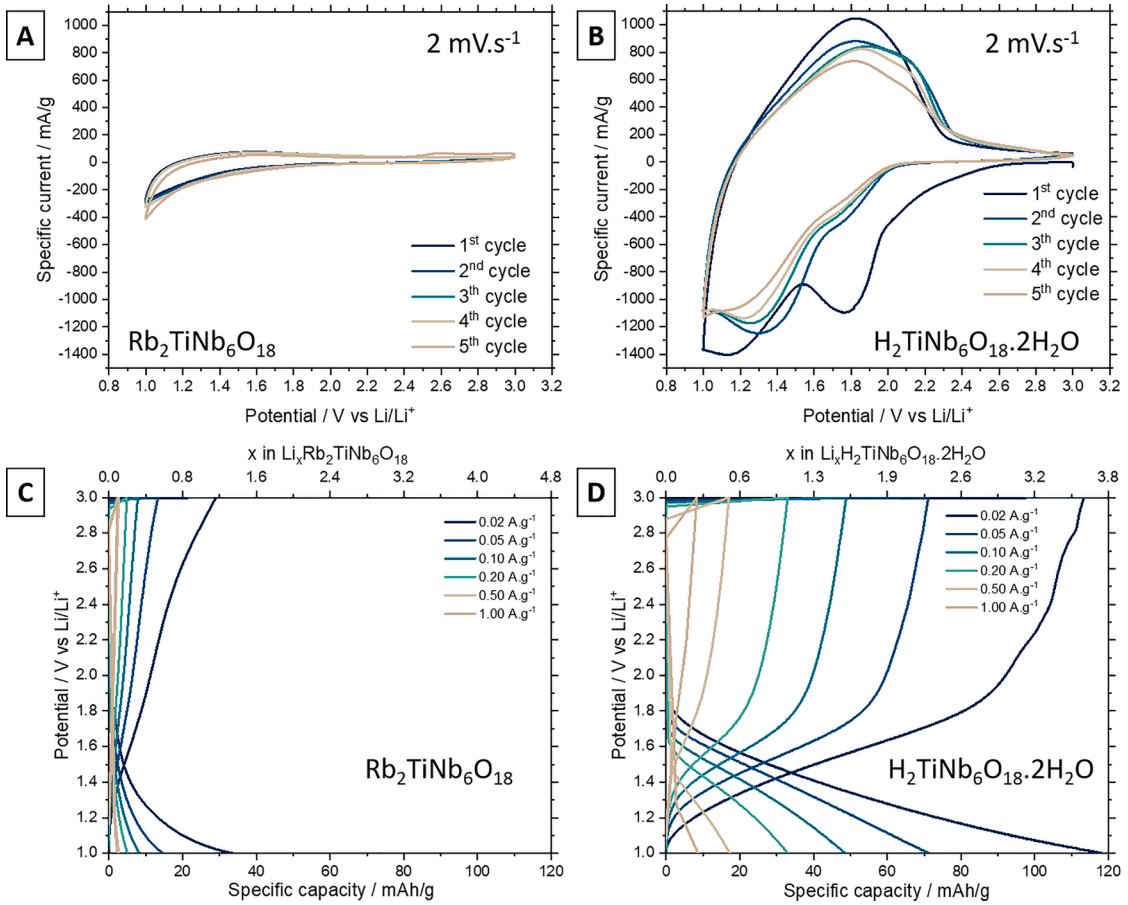

Fig. 3. A-B. Cyclic Voltammetry at 2 $mV.s^{-1}$ of $Rb_2TiNb_6O_{18}$ and $H_2TiNb_6O_{18}$ respectively. C-D. Charge and discharge curves at different current densities of $Rb_2TiNb_6O_{18}$ and $H_2TiNb_6O_{18}$ respectively.

high rate is probably due to the not favorable Li^+ diffusion between cages which limited the capacity at high current but also due to the large particles size which increases the diffusion length. Calculation of *b* value from CV at different scan rates (from 0.1 $mV.s^{-1}$ to 20 $mV.s^{-1}$) reveals a value close to 0.5 which seems to indicate that a diffusion-controlled process is controlling the insertion of ions in this type of structure [4,26–28]. For this reason, the synthesis of nanoparticles *via* soft chemistry can be an option to lower the diffusion length and increase the capacity of this type of structure at a higher cycling rate.

Fig. 4Ashows *in situ* XRD data collected during the first GCPL cycle of $H_2TiNb_6O_{18}{\cdot}2H_2O$ Note that the relative intensity of the peaks is different from that of the raw powder material, likely due to the preferential alignment of the anisotropic particles during electrode assembly. The absence of additional peak formation in Fig. 4.A. demonstrates that no phase change occurs upon electrode operation. Alternatively, a gradual shift of the peaks supports a solid solution mechanism, consistent with the linear GCPL profile observed before [29,30]. Additionally, the relatively small shift of the peaks indicates small volume variations

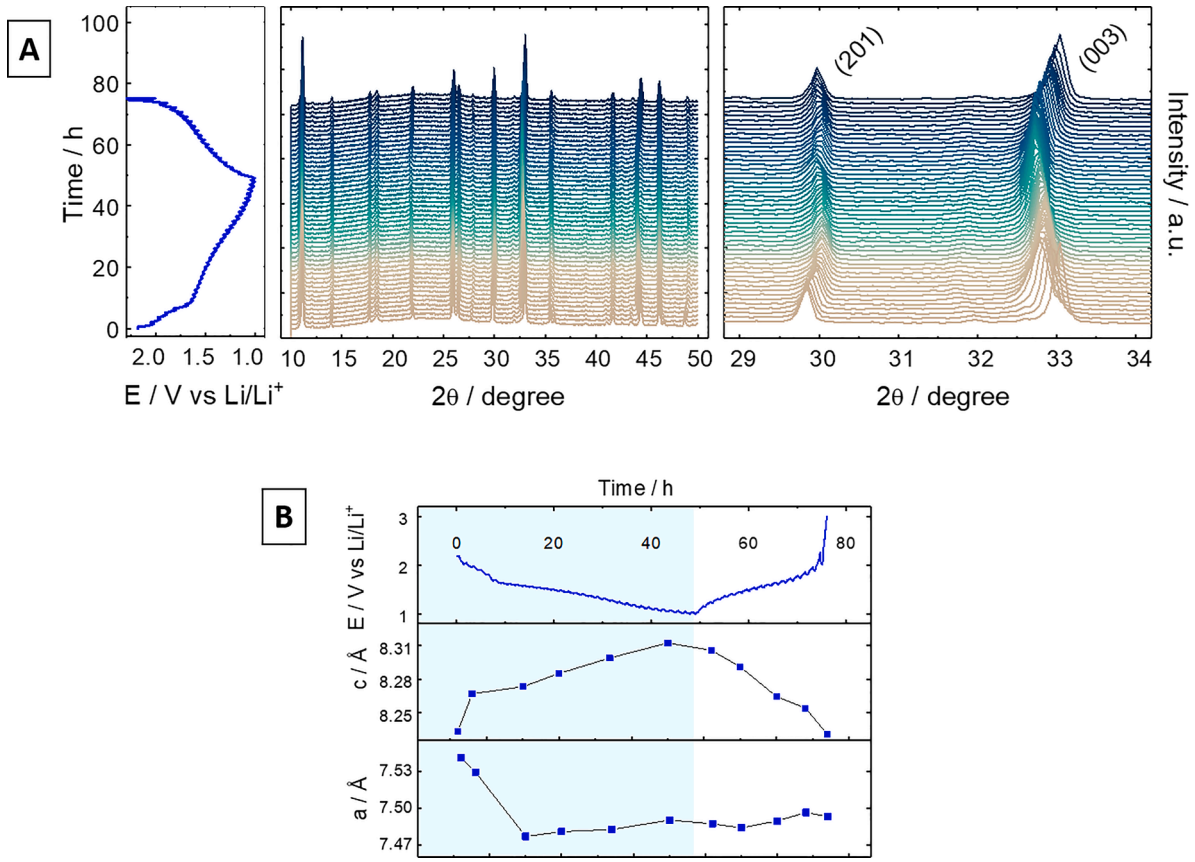

Fig. 4. A. *In situ* XRD of $H_2TiNb_6O_{18}$ cycled between 3.0 and 1.0 V at 0.005 A.g^{-1}. Charge /discharge and two 2θ ranges curves are shown. B. Evolution of cell parameters as a function of time during charge/discharge process.

[30,31]. This shift arises from a gradual change in the distances between atoms due to changes in the oxidation state of Nb and/ or Ti. Additionally, a more scrupulous observation shows the shifting of (00 *l*) reflections, while others remain almost constant, indicating a preferential lithium insertion along [0 0 1] direction.

Fig. 4B shows the unit cell evolution over the first discharge cycle. As calculated from Full Pattern Matching refinements, an initial pronounced decrease in the *a* parameter is observed. This effect is coincident with the removal of H_2O from the crystal structure at the beginning of the first reductive polarization. In fact, the water molecules have an influence on the stability of the structure as well as on electrostatic force of the protons with respect to the ($TiNb_6O_{18}$) skeleton. A hypothesis may be that the *a* parameter is modified to compensate the water molecule removal during the first cycle. After this initial change, no significant volume changes occur in the *a* parameter. Alternatively, a continuous increase in the *c* dimension over lithiation was determined, which is exemplified by the shifting behavior of the (0 0 3) reflection towards lower angles. Upon de-lithiation, a contraction in the *c* dimension is observed, while *a* stays relatively constant. Overall, the effect of volume expansion/contraction during the first cycle does not exceed 1%.

4. Conclusion

The motivation to find new negative electrode material for LIBs inspired the examination of unstudied structures previously reported in the literature. Here, $Rb_2Nb_6TiO_{18}$ was selected as a potential candidate based on its hexagonal tunnel structure, as well as the high amount of edge sharing octahedra. The investigation by Le Bail refinement and TEM has allowed a clear description of the materials. Moreover, for the first time, cationic exchange of $Rb_2Nb_6TiO_{18}$ with H_3O^+ was reported. Electrochemical measurements of $Rb_2Nb_6TiO_{18}$ electrode show a weak electrochemical activity, while Li ion insertion is clearly depicted in the protonated phase $H_2Nb_6TiO_{18}{\cdot}2H_2O$ A specific capacity of 118 mAh.g^{-1} is reported at 0.02 A.g^{-1} between 3 V and 1 V *vs* Li/Li$^+$. This impressive difference between $Rb_2TiNb_6O_{18}$ and $H_2TiNb_6O_{18}.2H_2O$ capacity highlights the importance of the nature of the cations in the ability to insert alkali ions in this type of structure. *In situ* XRD measurement showed no phase changes, indicating a solid-solution charge storage mechanism. Additionally, $H_2Nb_6TiO_{18}.2H_2O$ exhibits a minor volume expansion (1%) over Li$^+$ insertion along (0 0 1).

CRediT authorship contribution statement

Jeronimo Miranda: Investigation, Methodology, Writing – review & editing. **Etienne Le Calvez:** Investigation, Methodology, Writing – review & editing. **Richard Retoux:** TEM images. **Olivier Crosnier:** Conceptualization, Methodology, Supervision, Writing – review & editing. **Thierry Brousse:** Conceptualization, Methodology, Supervision, Writing – review & editing.

Declaration of Competing Interest

The authors declare that they have no known competing financial interests or personal relationships that could have appeared to influence the work reported in this paper.

Acknowledgements

The authors want to thank University of Nantes and NExT program for financial funding. JM thanks the Erasmus Mundus Joint Master Degree (MESC +) program and Institut des Matériaux de Nantes Jean Rouxel (IMN) for financial support. Eric Quarez is highly thanked for the

help during XRD pattern refinement. The authors thank the French National Research Agency for its financial support through the Labex STORE-EX LabexProject ANR-10LABX-76-01.

References

[1] A.M. Colclasure, A.R. Dunlop, S.E. Trask, B.J. Polzin, A.N. Jansen, K. Smith, Requirements for Enabling Extreme Fast Charging of High Energy Density Li-Ion Cells While Avoiding Lithium Plating, J. Electrochem. Soc. 166 (8) (2019) A1412–A1424, https://doi.org/10.1149/2.0451908jes.

[2] A. Burnham, E.J. Dufek, T. Stephens, J. Francfort, C. Michelbacher, R.B. Carlson, J. Zhang, R. Vijayagopal, F. Dias, M. Mohanpurkar, D. Scoffield, K. Hardy, M. Shirk, R. Hovsapian, S. Ahmed, I. Bloom, A.N. Jansen, M. Keyser, C. Kreuzer, A. Markel, A. Meintz, A. Pesaran, T.R. Tanim, Enabling Fast Charging – Infrastructure and Economic Considerations, J. Power Sources 367 (2017) 237–249, https://doi.org/10.1016/j.jpowsour.2017.06.079.

[3] M. Li, M. Feng, D. Luo, Z. Chen, Fast Charging Li-Ion Batteries for a New Era of Electric Vehicles, Cell Rep. Phys. Sci. 1 (10) (2020), 100212, https://doi.org/10.1016/j.xcrp.2020.100212.

[4] C. Choi, D.S. Ashby, D.M. Butts, R.H. DeBlock, Q. Wei, J. Lau, B. Dunn, Achieving High Energy Density and High Power Density with Pseudocapacitive Materials, Nat. Rev. Mater. 5 (1) (2020) 5–19, https://doi.org/10.1038/s41578-019-0142-z.

[5] M. Armand, J.-M. Tarascon, Building Better Batteries, Nature 451 (7179) (2008) 652–657, https://doi.org/10.1038/451652a.

[6] M.M. Thackeray, K. Amine, $Li_4Ti_5O_{12}$ Spinel Anodes, Nat. Energy 6 (6) (2021) 683, https://doi.org/10.1038/s41560-021-00829-2.

[7] K.J. Griffith, K.M. Wiaderek, G. Cibin, L.E. Marbella, C.P. Grey, Niobium Tungsten Oxides for High-Rate Lithium-Ion Energy Storage, Nature 559 (7715) (2018) 556–563, https://doi.org/10.1038/s41586-018-0347-0.

[8] V. Aravindan, J. Sundaramurthy, A. Jain, P.S. Kumar, W.C. Ling, S. Ramakrishna, M.P. Srinivasan, S. Madhavi, Unveiling $TiNb_2O_7$ as an Insertion Anode for Lithium Ion Capacitors with High Energy and Power Density, ChemSusChem 7 (7) (2014) 1858–1863, https://doi.org/10.1002/cssc.201400157.

[9] D. Butts, J. Schoiber, C. Choi, G.J. Redhammer, N. Hüsing, S. Donne, B. Dunn, Fe-Substituted Sodium B″-Al_2O_3 as a High-Rate Na-Ion Electrode, Chem. Mater. 33 (15) (2021) 6136–6145, https://doi.org/10.1021/acs.chemmater.1c01680.

[10] K.J. Griffith, I.D. Seymour, M.A. Hope, M.M. Butala, L.K. Lamontagne, M. B. Preefer, C.P. Koçer, G. Henkelman, A.J. Morris, M.J. Cliffe, S.E. Dutton, C. P. Grey, Ionic and Electronic Conduction in $TiNb_2O_7$, J. Am. Chem. Soc. 141 (42) (2019) 16706–16725, https://doi.org/10.1021/jacs.9b06669.

[11] A.S. Prakash, P. Manikandan, K. Ramesha, M. Sathiya, J.-M. Tarascon, A.K. Shukla, Solution-Combustion Synthesized Nanocrystalline $Li_4Ti_5O_{12}$ As High-Rate Performance Li-Ion Battery Anode, Chem. Mater. 22 (9) (2010) 2857–2863, https://doi.org/10.1021/cm100071z.

[12] V. Augustyn, J. Come, M.A. Lowe, J.W. Kim, P.-L. Taberna, S.H. Tolbert, H. D. Abruña, P. Simon, B. Dunn, High-Rate Electrochemical Energy Storage through Li^+ Intercalation Pseudocapacitance, Nat. Mater. 12 (6) (2013) 518–522.

[13] K.J. Griffith, A.C. Forse, J.M. Griffin, C.P. Grey, High-Rate Intercalation without Nanostructuring in Metastable Nb_2O_5 Bronze Phases, J. Am. Chem. Soc. 138 (28) (2016) 8888–8899, https://doi.org/10.1021/jacs.6b04345.

[14] G. Desgardin, C. Robert, D. Groult, B. Raveau, Une Nouvelle Famille Structurale: Les Titanoniobates et Titanotantalates $A_2Nb_6TiO_{18}$ et $A_2Ta_6TiO_{18}$, J. Solid State Chem. 22 (2) (1977) 101–111, https://doi.org/10.1016/0022-4596(77)90026-3.

[15] C. Michel, A. Guyomarc'h, B. Raveau, Nouveaux Echangeurs Cationiques Avec Une Structure a Tunnels Entrecroises: Les Oxydes A12M33O90 et al2M33O90, 12H2O, J. Solid State Chem. 22 (4) (1977) 393–403, https://doi.org/10.1016/0022-4596(77)90016-0.

[16] C. Michel, A. Guyomarc'h, B. Raveau, Nouveaux Échangeurs Cationiques Avec Une Structure à Tunnels Entrecroisés: Les Niobates et Tantalates A10M29.2O78 et al0M29.2O78·10H2O, J. Solid State Chem. 25 (3) (1978) 251–261, https://doi.org/10.1016/0022-4596(78)90110-X.

[17] G. Desgardin, C. Robert, B. Raveau, Etude Du Comportement Du Thallium Dans de Nouvelles Structures a Tunnels Entrecroises : Les Oxydes $Tl_2Nb_6TiO_{18}$ et $Tl_2Ta_6TiO_{18}$, Mater. Res. Bull. 13 (6) (1978) 621–626, https://doi.org/10.1016/0025-5408(78)90187-3.

[18] J.B. Leriche, S. Hamelet, J. Shu, M. Morcrette, C. Masquelier, G. Ouvrard, M. Zerrouki, P. Soudan, S. Belin, E. Elkaïm, F. Baudelet, An Electrochemical Cell for Operando Study of Lithium Batteries Using Synchrotron Radiation, J. Electrochem. Soc. 157 (5) (2010) A606, https://doi.org/10.1149/1.3355977.

[19] Y. Gogotsi, P. Simon, True Performance Metrics in Electrochemical Energy Storage, Science 334 (6058) (2011) 917, https://doi.org/10.1126/science.1213003.

[20] T.-Y. Chen, E.R. Maddrell, N.C. Hyatt, J.A. Hriljac, A Potential Wasteform for Cs Immobilization: Synthesis, Structure Determination, and Aqueous Durability of $Cs_2TiNb_6O_{18}$, Inorg. Chem. 55 (24) (2016) 12686–12695, https://doi.org/10.1021/acs.inorgchem.6b01826.

[21] M. Sato, J. Abo, T. Jin, M. Ohta, Structure and Ionic Conductivity of $MLaNb_2O_7$ (M= K, Na, Li, H), J. Alloys Compd. 192 (1–2) (1993) 81–83.

[22] J.-F. Colin, V. Pralong, M. Hervieu, V. Caignaert, B. Raveau, New Titanoniobates (Li, H_y)2$TiNb_O$5 and (Li, $_H$)3TiN_bO5: Synthesis, Structure and Properties. *J. Mater. Chem.* 18 (26) (2008) 3121–3128.

[23] Y.u. Yuan, H. Yu, X. Cheng, W. Ye, T. Liu, R. Zheng, N. Long, M. Shui, J. Shu, $H_{0.92}K_{0.08}TiNbO_5$ Nanowires Enabling High-Performance Lithium-Ion Uptake, ACS Appl. Mater. Interfaces 11 (9) (2019) 9136–9143, https://doi.org/10.1021/acsami.8b2181710.1021/acsami.8b21817.s001.

[24] C. Bohnke, O. Bohnke, J.L. Fourquet, Electrochemical Intercalation of Lithium into $LiLaNb_2O_7$ Perovskite, J. Electrochem. Soc. 144 (4) (1997) 1151.

[25] O.A. Drozhzhin, V.V. Grigoryev, A.M. Alekseeva, R.R. Samigullin, D.A. Aksyonov, O.V. Boytsova, D. Chernyshov, V.V. Shapovalov, A.A. Guda, A.V. Soldatov, K. J. Stevenson, A.M. Abakumov, E.V. Antipov, Revisited $Ti_2Nb_2O_9$ as an Anode Material for Advanced Li-Ion Batteries, ACS Appl. Mater. Interfaces 13 (47) (2021) 56366–56374.

[26] J.E.B. Randles, A Cathode Ray Polarograph. Part II.—The Current-Voltage Curves, Trans Faraday Soc 44 (0) (1948) 327–338, https://doi.org/10.1039/TF9484400327.

[27] A. Ševčík, Oscillographic Polarography with Periodical Triangular Voltage, Collect. Czechoslov. Chem. Commun. 13 (1948) 349–377.

[28] S. Fleischmann, J.B. Mitchell, R. Wang, C. Zhan, D. Jiang, V. Presser, V. Augustyn, Pseudocapacitance: From Fundamental Understanding to High Power Energy Storage Materials, Chem. Rev. 120 (14) (2020) 6738–6782, https://doi.org/10.1021/acs.chemrev.0c00170.

[29] J. Come, V. Augustyn, J.W. Kim, P. Rozier, P.-L. Taberna, P. Gogotsi, J.W. Long, B. Dunn, P. Simon, Electrochemical Kinetics of Nanostructured Nb_2O_5 Electrodes, J. Electrochem. Soc. 161 (5) (2014) A718–A725, https://doi.org/10.1149/2.040405jes.

[30] X. Yu, H. Pan, W. Wan, C. Ma, J. Bai, Q. Meng, S.N. Ehrlich, Y.-S. Hu, X.-Q. Yang, A Size-Dependent Sodium Storage Mechanism in $Li_4Ti_5O_{12}$ Investigated by a Novel Characterization Technique Combining in Situ X-Ray Diffraction and Chemical Sodiation, Nano Lett. 13 (10) (2013) 4721–4727, https://doi.org/10.1021/nl402263g.

[31] L. Zhao, H.-L. Pan, Y.-S. Hu, H. Li, L.-Q. Chen, Spinel Lithium Titanate ($Li_4Ti_5O_{12}$) as Novel Anode Material for Room-Temperature Sodium-Ion Battery, Chin. Phys. B 21 (2) (2012) 028201, https://doi.org/10.1088/1674-1056/21/2/028201.